USING FULLY COUPLED HYDRO-GEOMECHANICAL NUMERICAL TEST BED TO STUDY RESERVOIR STIMULATION WITH LOW HYDRAULIC PRESSURE

Pengcheng Fu, Scott M. Johnson, and Charles R. Carrigan

Atmospheric, Earth, and Energy Division, Lawrence Livermore National Laboratory
7000 East Ave., L-286
Livermore, CA 94550, USA
e-mail: fu4@llnl.gov

ABSTRACT

This paper documents our effort to use a fully coupled hydro-geomechanical numerical test bed to study using low hydraulic pressure to stimulate geothermal reservoirs with existing fracture network. In this low pressure stimulation strategy, fluid pressure is lower than the minimum *in situ* compressive stress, so the fractures are not completely open but permeability improvement can be achieved through shear dilation. The potential advantage of low pressure stimulation compared with high pressure stimulation is that a large fracture network instead of a single primary fracture can be stimulated. We found that in this low pressure regime, the coupling between the fluid phase and the rock solid phase becomes very simple, and the numerical model can achieve a low computational cost. Using this modified model, we study the behavior of a single fracture and a random fracture network.

INTRODUCTION

Geological formations in rocks with low initial permeability can be hydraulically stimulated to create enhanced (or engineered) geothermal reservoirs with enhanced permeability and thereby improved heat production efficiency (MIT study, 2006). The conceptual model for hydraulic stimulation that is most commonly referred to depicts the following process. When fluid pressure exceeds the minimum principal stress in the rock formation, new hydraulic fractures initiate and propagate along the plane that is perpendicular to the minimum principal stress direction. These new hydraulic fractures will intersect existing natural fractures in the formation and form a interconnected fracture network, through which fluid in the production phase can flow from the injection well to the production well(s) and bring heat from the hot rocks covered by this network.

A concern over the process described in this conceptual model is that once a hydraulic fracture (termed primary fracture herein) is opened, the conductivity along this fracture from the injection point to the fracture front is much higher than the neighboring fractures that are still closed. Meanwhile, the high fluid pressure in this open fracture creates a "stress shadow" around this fracture, which increases the rock matrix compressive stress experienced by neighbor fractures. The direct consequence of these two effects is that this open fracture will continue to grow at a relatively high rate, thereby further strengthening these effects, whereas the neighbor closed fractures may never be able to open and subsequently compete with the primary fracture. This is true regardless whether the primary fracture is a newly created hydraulic fracture or an existing fracture that happens to be oriented normal to the minimum principal stress. In this scenario, only one fracture (the primary fracture) can be stimulated. Even though it is possible to obtain high permeability between the injection well and the production well through this primary fracture, heat in a small volume in the reservoir around this fracture can be harvested, which is highly undesired for enhanced geothermal system (EGS) stimulation. It is possible to stimulate multiple fractures and create interconnected fracture network using technologies such as horizontal drilling with staged fracking, but such technologies are expensive and more applicable to shale gas production than to EGS.

An alternative stimulation strategy is to stimulate the reservoir at a fluid pressure lower than the minimum principal stress in the rock matrix. No new fractures will be created and none of the existing fractures will be completely open. In this scenario, instead of stimulate a single fracture, the fracture network which must already be interconnected prior to the stimulation will be stimulated by "hydro-shearing" (Willis-Richards et al., 1996). This paper investigates the mechanisms of low pressure hydraulic

stimulation using a fully coupled hydro-geomechanical numerical test bed developed at the Lawrence Livermore National Laboratory. The numerical algorithms in this numerical test bed, which originally focuses on high-pressure hydraulic fracturing, have been documented elsewhere (Johnson and Morris, 2009; Fu et al., 2011). In this paper, we describe the modifications to the original algorithms that enable high-efficiency simulation of low pressure stimulation in this paper, as well as various numerical examples on low pressure stimulation.

STRESS SHADOWING CONSIDERATION

First, we quantitatively evaluate the evolution of stress shadowing, namely the increase of rock matrix stress as fluid pressure in a fracture increases. Consider an infinite array of parallel fractures with infinite length as a highly idealized scenario that enables a closed-form solution to be obtained, as illustrated in Figure 1. The distance between any two neighboring fractures is H. Initially the fluid pressure in these fractures is $P_F=0$ and the rock matrix stress normal to the fractures is σ_{Mi}. As the fractures are simultaneously pressurized with fluid, they will begin to dilate and the rock matrix stress σ_M will increase accordingly. The effective normal stress along these fractures

$$\sigma'_J = \begin{cases} \sigma_M - P_F & \text{if } \sigma_M > P_F \\ 0 & \text{otherwise} \end{cases} \quad (1)$$
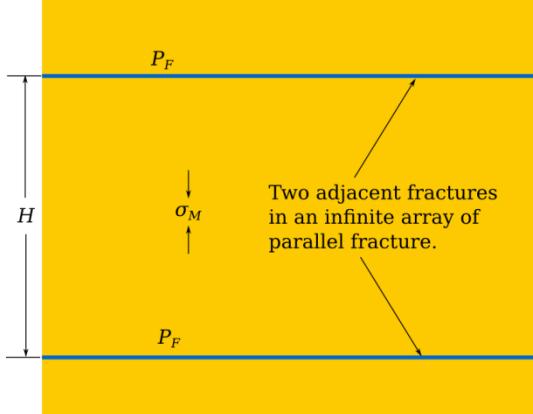

Figure 1: Two adjacent fractures in an infinite array of parallel fractures.

Note that σ_M is not a constant, but a function of σ_{Mi} and P_F. Assume under the initial condition (effective normal stress being σ_{Mi}) the mechanical aperture width is w_i; at arbitrary effective joint stress σ'_J the mechanical aperture width becomes w. We define the secant unloading joint stiffness to be

$$\bar{k}_n = \frac{\sigma_{MJ} - \sigma'_J}{w(\sigma'_J) - w_i} \quad (2)$$

The normal stiffness of a joint k_n is conventionally defined using the zero-normal stress state as the reference state, whereas we use the zero-fluid pressure state as the reference. The compression experienced by the rock body between two neighboring fractures due to a matrix stress increase from σ_{Mi} to σ_M should be the same as the joint dilation due to the corresponding effective stress change from σ_{Mi} to σ'_J, namely

$$w(\sigma'_J) - w_i = \frac{(\sigma_M - \sigma_{Mi})H}{E'} \quad (3)$$

where E' is the confined stiffness of the rock matrix as

$$E' = \frac{E(1-\nu)}{(1-2\nu)(1+\nu)} \quad (4)$$

with E and ν being the Young's modulus and Poisson's ratio of the rock, respectively. We introduce a length scale

$$\bar{h}_n = E'/\bar{k}_n \quad (5)$$

so that the closure of the joint between the reference stress state and the current effective stress state is the same as the compression of a layer of virtual rock mass of thickness $\bar{k}_n$ experiencing the same stress change.

By plugging equations (1) and (2) into equation (3), we can obtain the increment of rock matrix stress $\Delta\sigma_M = \sigma_M - \sigma_{Mi}$ as

$$\Delta\sigma_M = \begin{cases} P_F/(1 + H/\bar{h}_n) & \text{if } P_F \leq \sigma_{Mi}(1 + \bar{h}_n/H) \\ P_F - \sigma_{Mi} & \text{otherwise} \end{cases} \quad (6)$$

which indicates that the fracture will be completely open if the fluid pressure is higher than a threshold value of $\sigma_{Mi}(1 + \bar{h}_n/H)$. When the fracture is still partially closed, the rock matrix stress increment is only a small portion of the fluid pressure increment. A survey of rock mechanics literature (e.g. Bandis et al., 1983; Barton et al., 1985; Cook, 1992) found that $\bar{h}_n$ is generally within the range between tens to hundreds of millimeters for interlocked rocks compressed with a stress level typical of hydraulic stimulation applications. If the fracture spacing is in the range of a few meters to tens of meters, then the rock matrix stress increment is a relatively small percentage of the fluid pressure increment. Therefore, the stress shadowing effects for partially closed fractures can generally be ignored. We term this scenario "joint stiffness-dominated" regime for fracture flow.

On the other hand, however, as the fluid pressure exceeds the threshold value and the fractures are completely open, the opening of the fracture will not be governed by joint stiffness, but by the deformation

in the rock matrix instead. Under this condition, the stress shadowing effects mentioned in the first section dictates that a primary fracture will emerge and suppress the pressure propagation in neighbor fractures.

COUPLING JOINT MODEL WITH FLOW SOLVER

In order to investigate fluid pressure propagation in the joint stiffness-dominated regime in an arbitrary fracture network, we use the numerical model for hydraulic fracturing developed at the Lawrence Livermore National Laboratory (LLNL). This fully coupled hydro-geomechanical model has been described elsewhere (Fu et al., 2011) and will not be repeated here. However, the original model was formulated for the scenarios where the fractures are completely open. To simulate the cases with partially closed fractures, some modifications are necessary. The weak stress shadowing effect allows us to directly incorporate joint closure models into the finite volume flow solver.

Fractures are discretized into interconnected flow cells in the flow solver. The permeability of each flow cell is a function of the hydraulic aperture width and the fluid storage volume of a cell is related to the mechanical aperture size. It is well known that the hydraulic aperture width is highly correlated with the mechanical aperture size as effective stress evolves, with the former generally smaller than the latter (Cook, 1992). However, their difference is ignored in this preliminary study. In each time step of solving the network flow, the fluid mass into and out of each flow cell is calculated and subsequently, the fluid mass in each cell is updated. Fluid pressure in each cell is calculated using the following equation-of-state

$$P_F = \begin{cases} K_F\left(1 - \dfrac{\rho_{ref} L_C w}{m_C}\right) & \text{if } m_C / L_C w \geq \rho_{ref} \\ P_{vap} & \text{if } m_C / L_C w < \rho_{ref} \end{cases} \qquad (7)$$

where K_f is the bulk modulus of the fluid; ρ_{ref} is the reference density of this fluid, namely the density at zero or the datum pressure; L_c is the length (area in 3D) of the fluid cell and w is the aperture width, so $L_c w$ is the fluid storage volume of the cell; m_c is the fluid mass in this cell; P_{vap} is the temperature-dependent vapor pressure of this fluid which can be considered to be zero for the purpose of hydraulic stimulation modeling as the pumping pressure is many orders of magnitude higher than the vapor pressure. In the original model, the aperture width is

calculated based on the deformation of the rock mass through a finite element solver. In the current study, instead we adopt the well known closure model by Bandis et al. (1983), which relates the aperture width w and joint effective normal stress as

$$\sigma' = \frac{w_{max} - w}{a - b(w_{max} - w)} \qquad (8)$$

where w_{max} is the aperture width at the zero-effective stress state, which is essentially the maximum joint closure in the original joint model; a and b are two material-specific constant. We plug equations (7) and (8) into equation (1) and obtain

$$\sigma_M - K_F\left(1 - \frac{\rho_{ref} L_C w}{m_C}\right) = \frac{w_{max} - w}{a - b(w_{max} - w)} \qquad (9)$$

which can be solved as

$$w = w_{max} - \frac{Aa + Bb + 1 - [(Aa + Bb + 1)^2 - 4AaBb]^{0.5}}{2Ab} \qquad (10)$$

where $A=K_F\rho_{ref}L_C/m_C$ and $B=\sigma_M-K_F+Aw_{max}$ are two constants to simplify the expression of the equations. With this equation, we can directly calculate the aperture width at each time step from the updated fluid mass and then obtain the fluid pressure using equation (7). The finite element solid solver is not required for joint stiffness-dominated fluid flow.

FLOW IN A SINGLE FRACTURE

We investigate fluid flow in a single fracture in this section. Because the strong coupling between fluid pressure, aperture volume, and aperture permeability, closed-form solutions cannot be derived.

A 100 meter long straight fracture is considered and it is discretized into 1,000 flow cells with $L_C=0.1$ m. In the initial condition where no fluid exists in the fracture, the normal stress along the fracture $\sigma_n=10$ and we ignore the total normal stress change due to pressurization of the fracture. In this state, the aperture width $w_i=0.01$ mm whereas $w_{max}=0.1$ mm corresponding to the zero-effective stress state. The closing behavior of the fracture is anchored by these two states and we can back-calculate the two constants in the joint model as

$$a = w_{max}\frac{w_{max} - w_i}{\sigma_n w_i} \text{ and } b = \frac{w_{max} - w_i}{\sigma_n w_i} \qquad (11)$$

The dynamic viscosity, bulk modulus (K_F), and reference density (ρ_{ref}) of the fluid are 0.001 Pa·s, 2.2 GPa, and 1,000 kg/m^3, respectively. All the above parameters remain the same for all the numerical examples in this paper unless stated otherwise.

In the baseline scenario, we start pumping fluid with pressure P_{F0}=10 MPa into the fracture at time t=0. This is also the highest fluid pressure allowed by the joint stiffness-dominated regime. The length of the fracture that is pressurized by fluid L_F as a function of t is shown in Figure 2(a). A regression analysis finds that L_F is linearly proportion to the square root of t, with the regression equation and a perfect R^2 value shown in the figure. For an ideal case where the aperture width is a constant regardless of the fluid pressure, a closed-form solution exist between L_F and t as

$$L_F = w\left(\frac{P_0 t}{6\mu}\right)^{1/2} \tag{12}$$

which also indicates that L_F is a linear function of the square root of t. In Figure 2(a), two scenarios with pressure-independent aperture widths 0.1 mm and 0.01 mm are plotted. Since these two aperture widths are the upper and lower bounds of the aperture width in the baseline case, it is not surprising to see the propagation speed of the baseline case is somewhere between these two ideal cases.
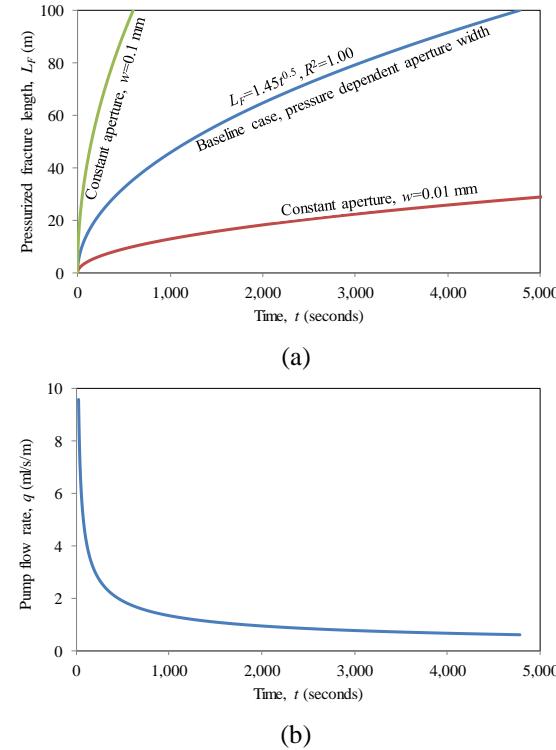

(a)

(b)

Figure 2: Numerical simulation results for the baseline single fracture. (a).

The flow rate q at the pumping end of the fracture decreases as the fluid front propagates, as shown in Figure 2(b). This phenomenon has an important implication for the stimulation of a fracture network. It indicates that as the stimulation progresses, it will be more and more difficult to pump fluid into a single fracture. The flow tends to find alternative route, thereby stimulating other fractures in the network. On the other hand, if an open primary fracture has developed, the flow rate into this fracture increases as this fracture grows if the pump pressure remains constant. This single fracture will consume most of the fluid volume and make the stimulation of other fractures more difficult.

Two more simulations for the same single fracture but with lower pumping pressures, 5 MPa and 2 MPa, were performed and the results are shown in Figure 3. The effect of pumping pressure on the fluid front propagation rate is very significant. For all the three pumping pressures, L_F is always a linear function of the square root of time. We also implemented some other forms of the relationship between the effective normal stress and the aperture width in addition to the Bandis-Barton model, and found that this square root grow rate relationship is always valid.
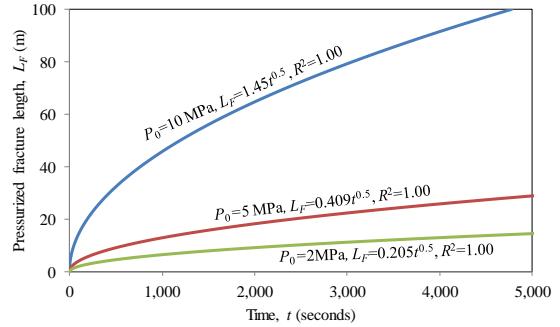

Figure 3: The effects of pumping pressure P_0 on the growth rate of L_F.

SELF-PROPPING THROUGH SHEAR DILATION

It is believed that a fracture network can be stimulated by the mechanism of shear dilation under the following conditions: 1) There exists significant shear stress long the fractures; and 2) the fluid pressure is high enough to induce shear slipping of the fractures as a result of the reduced effective stress. Predicting the amount of shear dilation is a challenging task, primarily due to the lack of experiment data that enable characterization of joint behaviors along the complex stress paths associated with hydraulic stimulation and the subsequent drawdown. The following simple phenomenological

empirical model is used in this study to represent the most important shear dilation behaviors associated with low pressure stimulation.

We introduce a variable, termed the stimulation factor S to quantify the extent to which a fracture has been stimulated through shear dilation. The aperture width is a function of not only the compressive effective stress σ', but also this stimulation factor S. If we assume the effects of σ' and those of S can be decoupled, S becomes a multiplier of the original joint model as

$$w = w(\sigma', S) = Sw(\sigma') \qquad (13)$$

In the unstimulated state, $S=S_0=1$. We denote the three parameters in the joint model in this state as w_{max0}, a_0 and b_0, and the evolution of these parameters with S is as $w_{max} = w_{max\,0}S$ and $a = a_0 S$ while b is a constant as $b=b_0$. We define the "excessive" shear stress along a fracture to be $\tau'=\tau_0-\sigma'\mu$, where τ_0 is the shear stress along the fracture in the initial state without hydraulic pressure and μ is coefficient of friction of the fracture. The stimulation factor S is assumed to be related to the greatest excessive shear stress τ'_{max} ever achieved by the fracture

$$S = \begin{cases} 1 + \tau'_{max}\ (S_{max} - 1)\,/\,\tau'_s & \text{if } \tau'\tau'_{max} < \tau'_s \\ S_{max} & \text{otherwise} \end{cases} \qquad (14)$$

where S_{max} is the upper limit of S and S reaches S_{max} at excessive shear stress τ'_s. The above formulation dictates that an increase of the excessive shear stress can induce increase of S, but a decrease of τ' has no effect on S. In other words, the stimulation effects induced by the increase of fluid pressure will not be reversed when the pressure decreases after the stimulation. However, the aperture size is still a function of the effective stress as dictated by equation (8). The main effect of stimulation by shear dilation is to change the values of the constants in equation (8).

NUMERICAL EXAMPLE: STIMULATION OF A NATURAL FRACTURE NETWORK

In this section, we exercise the numerical model on a virtual reservoir. As shown in Figure 4, the simulation domain is 320 m wide (x from -160 m to 160 m) and 240 m tall (y from 0 to 240 m). There are two sets of joints (existing natural fractures) in this reservoir. The horizontal set has orientation angles with a uniform distribution between 10° and 30° where as the vertical set has orientation angles between 80° and 100°. Note that this 2D simulation domain should be considered as a plan view of the reservoir, so the term "vertical" refers to the direction within the image, not the vertical direction in a 3D

space. All the fractures have lengths between 20 m and 60 m and the total length of fractures in the two sets are 8,300 m and 8,700 m respectively. The injection well is located near the middle point of the lower boundary of the domain as shown in Figure 4, so the simulation is on a half of the reservoir. The location of the production well is shown in Figure 4. The far field *in situ* stress applied is σ_{xx}=10 MPa, σ_{yy}=14 MPa, and σ_{xy}=0. Since the fractures usually do not exactly align with the coordinate system, shear stress dependent on the orientation angle exists along these fractures. Joint model parameters used are shown in Table 1 and parameters for the fluid phase are the same as the numerical examples for single fractures..

Table 1: Model parameters used in this study.

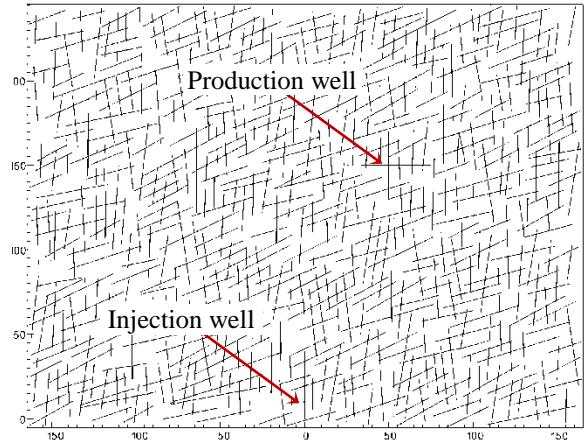| Parameter	Value
w_{max0}	0.2 mm
w_{i0}	0.02 mm
t'_s	3 MPa
S_{max}	3.0
μ	0.7

Figure 4: The effects of pumping pressure P_0 on the growth rate of L_F.

The injection pressure at the injection well is 10 MPa, the same as the minimal principal stress. The portions of the fracture network that is pressurized (with non-zero fluid fracture) at 20,000 seconds (5.6 hours) and 100,000 seconds (28 hours) after the injection has started are shown in Figure 5.
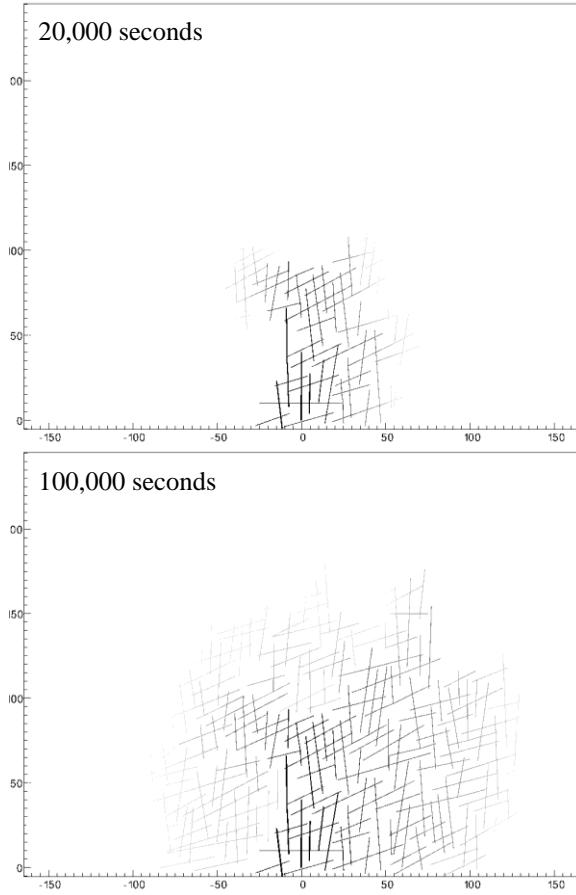
Figure 5: Pressurized fracture network 20,000 and 100,000 seconds after stimulation.

We simulate four scenarios (A to D) that share the same stimulation process in the first 100,000 seconds as described above but with different subsequent operations after 100,000 seconds. For cases A through C, we start pumping into the production well with 10 MPa fluid pressure from 100,000 seconds to 125,000 seconds. The objective is to stimulate the fractures near the production well. The difference between these three cases is the back pressure we use in the production state, being 0, 2 MPa, and 4 MPa for cases A, B, and C, respectively. A higher back pressure can increase the aperture width and permeability in the near-well region but on the other hand, it also decreases the pressure gradient from the injection well and the production well. In case D, we do not stimulate the region around the production well but directly apply 4 MPa of back pressure at 100,000 seconds.

The flow rates at the two wells for case A are shown in Figure 6. Negative flow rate means flow from the well into the reservoir and positive value means flow from the reservoir to the well. Because this is a 2D model, the flow rate is for unit-thickness reservoir. From the beginning of the stimulation (t=0) to

100,000 seconds, the absolute flow rate at the injection well continues to decreases, similar to what the single fracture model has shown. The fluid front reaches the production well at approximately 50,000 seconds, and fluid starts to flow out from that well, which is an artifact of the zero-pressure boundary condition given at the well. Fluid flow into the production well between t=100,000 and t=125,000 seconds during the stimulation through the production well. Once we lower the pressure to the back pressure (0 for case A), fluid starts to flow back into the well. The flow rate in the beginning is high due to the high pressure that has built up during the production well stimulation, and it soon reaches a relatively steady level when most of the fluid is supplied from the injection well. We terminate the simulation at 300,000 seconds because the fluid front has reaches the boundary of the simulation domain. At this moment, the injection rate is still slowly decreasing and the production rate is slowly increasing. The flow rate at t=300,000 seconds for all four scenarios are summarized in Table 2.
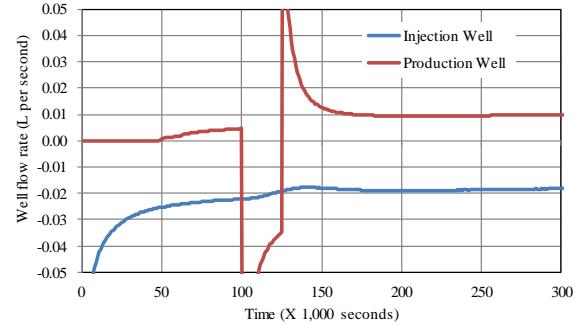

Figure 6: Flow rate at the two wells in scenario A.

Table 2: *Absolute flow rate at t=300,000 seconds.*

Scenario	Injection (L/s)	Production (L/s)
A	0.0183	0.00991
B	0.0197	0.00913
C	0.0197	0.00779
D	0.0193	0.00720

The fluid recovery ratios (production flow rate divided by injection rate) for the four scenarios are 54%, 46%, 40%, and 37%, respectively. The benefit of production well stimulation is apparent, but the back pressure seems to not only reduces flow rate but also decreases recovery rate. Placing more production wells should increase the recovery ratio, but this is to be studied in the future.

SUMMARY

In this study, we investigate the use of a numerical test bed to study the stimulation of existing fracture

networks with relatively low hydraulic pressure. We found that in this regime, the coupling between the flow and the solid phase can be considered local and the numerical model can be greatly simplified. The results show that low pressure stimulation can indeed stimulate the entire network, instead of propping a primary fracture as in high pressure stimulation. This paper only documents our initial effort along this path, and more realistic scenarios are to be studied.

REFERENCES

The Future of Geothermal Energy: Impact of Enhanced Geothermal Systems (EGS) on the United States in the 21st Century (2006). Research report by an MIT-led interdisciplinary panel.

Barton, N., Bandis, S., Bakhtar, K. (1985), "Strength, deformation and conductivity coupling of rock joints," *International Journal of Rock Mechanics and Mining Sciences & Geomechanics Abstracts*, 22(3), 121-140.

Bandis, S., Lumsden, A., Barton, N. (1983), "Fundamentals of rock joint deformation," *International Journal of Rock Mechanics and Mining Sciences & Geomechanics Abstracts*, 20(6), 249-268.

Cook, N.G.W. (1992), "Natural joints in rock: Mechanical, hydraulic and seismic behaviour and properties under normal stress," *International Journal of Rock Mechanics and Mining Sciences & Geomechanics Abstracts*, 29(3),198-223..

Fu, P., Johnson, S.M., Hao, Y., and Carrigan, C.R. (2011), "Fully coupled geomechanics and discrete flow network modeling of hydraulic fracturing for geothermal applications." *The 36th Stanford Geothermal Workshop*, Jan. 31 – Feb. 2, 2011, Stanford, CA.

Johnson, S.M., and Morris, J.P. (2009), "Modeling hydraulic fracturing for carbon sequestration applications," *the 43rd US Rock Mechanics Symposium and the 4th US-Canada Rock Mechanics Symposium*, Asheville, NC, ARMA 09-30.

Willis-Richards, J., Watanabe, K., Takahashi, H. (1996), "Progress toward a stochastic rock mechanics model of engineered geothermal systems," *Journal of Geophysical Research*, 101(B8),17481–17.